



Faster Acquisition and Improved Image Quality of T2-Weighted Dixon Breast MRI at 3T Using Deep Learning: A Prospective Study

Caroline Wilpert¹, Hannah Schneider¹, Alexander Rau^{1,2}, Maximilian Frederic Russe¹, Benedict Oerther¹, Ralph Strecker^{3,4}, Marcel Dominic Nickel³, Elisabeth Weiland³, Alexa Haeger^{5,6}, Matthias Benndorf¹, Thomas Mayrhofer^{7,8}, Jakob Weiss¹, Fabian Bamberg¹, Marisa Windfuhr-Blum¹, Jakob Neubauer¹

¹Department of Diagnostic and Interventional Radiology, University Medical Center Freiburg, Faculty of Medicine, University of Freiburg, Freiburg, Germany

²Department of Neuroradiology, University Medical Center Freiburg, Faculty of Medicine, University of Freiburg, Freiburg, Germany

³MR Application Predevelopment, Siemens Healthcare GmbH, Erlangen, Germany

⁴EMA Scientific Partnerships, Siemens Healthcare GmbH, Erlangen, Germany

⁵Department of Neurology, RWTH Aachen University, Aachen, Germany

⁶JARA-BRAIN Institute Molecular Neuroscience and Neuroimaging, Forschungszentrum Jülich GmbH and RWTH Aachen University, Aachen, Germany

⁷School of Business Studies, Stralsund University of Applied Sciences, Stralsund, Germany

⁸Cardiovascular Imaging Research Center, Department of Radiology, Massachusetts General Hospital and Harvard Medical School, Boston, MA, USA

Objective: The aim of this study was to compare image quality features and lesion characteristics between a faster deep learning (DL) reconstructed T2-weighted (T2-w) fast spin-echo (FSE) Dixon sequence with super-resolution (T2_{DL}) and a conventional T2-w FSE Dixon sequence (T2_{STD}) for breast magnetic resonance imaging (MRI).

Materials and Methods: This prospective study was conducted between November 2022 and April 2023 using a 3T scanner. Both T2_{DL} and T2_{STD} sequences were acquired for each patient. Quantitative analysis was based on region-of-interest (ROI) measurements of signal-to-noise ratio (SNR) and contrast-to-noise ratio (CNR). Qualitative analysis was performed independently by two radiologists using Likert scales to evaluate various image quality features, morphology, and diagnostic confidence for cysts and breast cancers. Reader preference between T2_{DL} and T2_{STD} was assessed via side-by-side comparison, and inter-reader reliability was also analyzed.

Results: Total of 151 women were enrolled, with 140 women (mean age: 52 ± 14 years; 85 cysts and 31 breast cancers) included in the final analysis. The acquisition time was 110 s ± 0 for T2_{DL} compared to 266 s ± 0 for T2_{STD}. SNR and CNR were significantly higher in T2_{DL} ($P < 0.001$). T2_{DL} was associated with higher image quality scores, reduced noise, and fewer artifacts ($P < 0.001$). All evaluated anatomical regions (breast and axilla), breast implants, and bone margins were rated higher in T2_{DL} ($P \leq 0.008$), except for bone marrow, which scored higher in T2_{STD} ($P < 0.001$). Scores for conspicuity, sharpness/margins, and microstructure of cysts and breast cancers were higher in T2_{DL} ($P \leq 0.002$). Diagnostic confidence for cysts was improved with T2_{DL} ($P < 0.001$). Readers significantly preferred T2_{DL} over T2_{STD} in side-by-side comparisons ($P < 0.001$).

Conclusion: T2_{DL} effectively corrected for SNR loss caused by accelerated image acquisition and provided a 58% reduction in acquisition time compared to T2_{STD}. This led to fewer artifacts and improved overall image quality. Thus, T2_{DL} is feasible and has the potential to replace conventional T2-w sequences for breast MRI examinations.

Keywords: MRI methods; Artificial neural network/machine learning; Breast; Quality assurance/control and improvement; Cancer

Received: December 29, 2023 **Revised:** October 15, 2024 **Accepted:** October 15, 2024

Corresponding author: Caroline Wilpert, MD, Department of Diagnostic and Interventional Radiology, University Medical Center Freiburg, Faculty of Medicine, University of Freiburg, 55 Hugstetterstreet, Freiburg 79106, Germany

• E-mail: caroline.wilpert@uniklinik-freiburg.de

This is an Open Access article distributed under the terms of the Creative Commons Attribution Non-Commercial License (<https://creativecommons.org/licenses/by-nc/4.0>) which permits unrestricted non-commercial use, distribution, and reproduction in any medium, provided the original work is properly cited.

INTRODUCTION

Deep learning (DL) models have recently been introduced to assist in diagnostic and segmentation tasks, showing significant improvements in the image quality and acquisition time of T2-weighted (T2-w) magnetic resonance imaging (MRI) sequences [1,2]. DL-based image reconstruction methods have demonstrated superior image quality and maintained or even improved signal-to-noise ratio (SNR) across various sequence types, anatomical structures, and organ systems [3-7]. Although there is a high demand for breast MRI, which could be met by improvements in acquisition time, the use of DL reconstruction for breast MRI has not been well studied.

In addition to analyzing breast lesions using contrast-enhanced dynamic T1-w sequences, T2-w sequences provide valuable anatomical contrast, assist in evaluating masses, and can help narrow the differential diagnosis. T2-w imaging can improve the specificity of breast MRI, reducing the risk of false positives [8]. Breast MRI performed at 3T field strength is superior to 1.5T in terms of faster acquisition and higher SNR, enhancing the visualization of morphological features [9]. The main technical issue of B0 field inhomogeneities at 3T when using conventional fat saturation can be addressed using the Dixon method, which offers uniform fat suppression [10]. The Dixon method has the advantage of simultaneously obtaining fluid- and fat-sensitive sequences, which can increase specificity for detecting fat-containing masses, such as fibroadenomas, fat necrosis, and lymph nodes [11]. Despite the disadvantages of swapping artifacts [12] and longer acquisition times associated with the Dixon technique [13], T2-w Dixon sequences have demonstrated superior fat suppression compared to standard spectral fat suppression techniques in breast imaging [12,14], and have been integrated into abbreviated protocols [15,16].

Acquisition times can be reduced by parallel imaging, compressed sensing (CS), or interpolation techniques [17]. DL-based image reconstruction has been shown to compensate for the lower SNR caused by parallel imaging techniques, achieved by undersampling k-space data, which allows for fewer iterations and thus faster acquisition [18]. The combination of a DL-reconstructed T2-w Dixon sequence using iterative denoising [19] and super-resolution (SR) networks [1] is promising. Given that T2-w imaging is associated with relatively long acquisition times, further optimization could improve the efficiency of breast MRI. As

DL reconstruction may mask small lesions [20], it is crucial to evaluate DL applications in detail.

The objective of this study was to evaluate whether deep learning reconstructed T2-weighted Dixon with super-resolution ($T2_{DL}$) improves acquisition time, quantitative and qualitative image quality characteristics, and diagnostic confidence for cysts and breast cancers.

MATERIALS AND METHODS

Study Design

This prospective, mono-institutional study was conducted between November 2022 and April 2023 on participants presenting for breast MRI for screening, follow-up, staging, or diagnostic clarification of results. The inclusion criteria were age over 18 years and no allergies to contrast agents, devices unsuitable for MRI, impaired renal function, or pregnancy/lactation period. Of the 237 women offered participation, 151 agreed and gave written informed consent before examinations with a standardized protocol were performed. Procedures are in line with the Declaration of Helsinki, were approved by the Institutional Review Board of the University of Freiburg (IRB No. EK22-1185), and are registered in the German Clinical Trials Register (DRKS-ID: DRKS00029550). Subsequent exclusion criteria included an incomplete study protocol at 3T MRI, technical defects, and incomplete histopathological documentation for breast cancers. A pseudonymized design was used to obtain additional information in cases of proven malignancy, which was blinded for the readings. See study enrollment in Figure 1.

MRI Acquisition Parameters

MRI was performed using a 3T scanner (MAGNETOM Vida, Siemens Healthcare, Erlangen, Germany) with an 18-channel breast coil (Siemens Healthcare). Prior to a standard dynamic breast MRI protocol with pre- and three post-contrast-enhanced T1-w fast spin-echo (FSE) Dixon series (Gadoteridol 0.1 mL/kg body weight; Bracco Imaging; sequence parameters: echo time: 2.46, repetition time: 5.96, flip angle: 8, slice thickness: 2 mm, Matrix: 576 x 576), a standard T2-weighted fast spin-echo Dixon sequence ($T2_{STD}$) and a research application package of a DL-reconstructed T2-w FSE Dixon with SR ($T2_{DL}$) were acquired. Regular undersampling was implemented with generalized autocalibrating partially parallel acquisition using the Parallel Imaging Technique. The acceleration factors were 4 for $T2_{DL}$ and 2 for $T2_{STD}$. Matrix size and spatial resolution

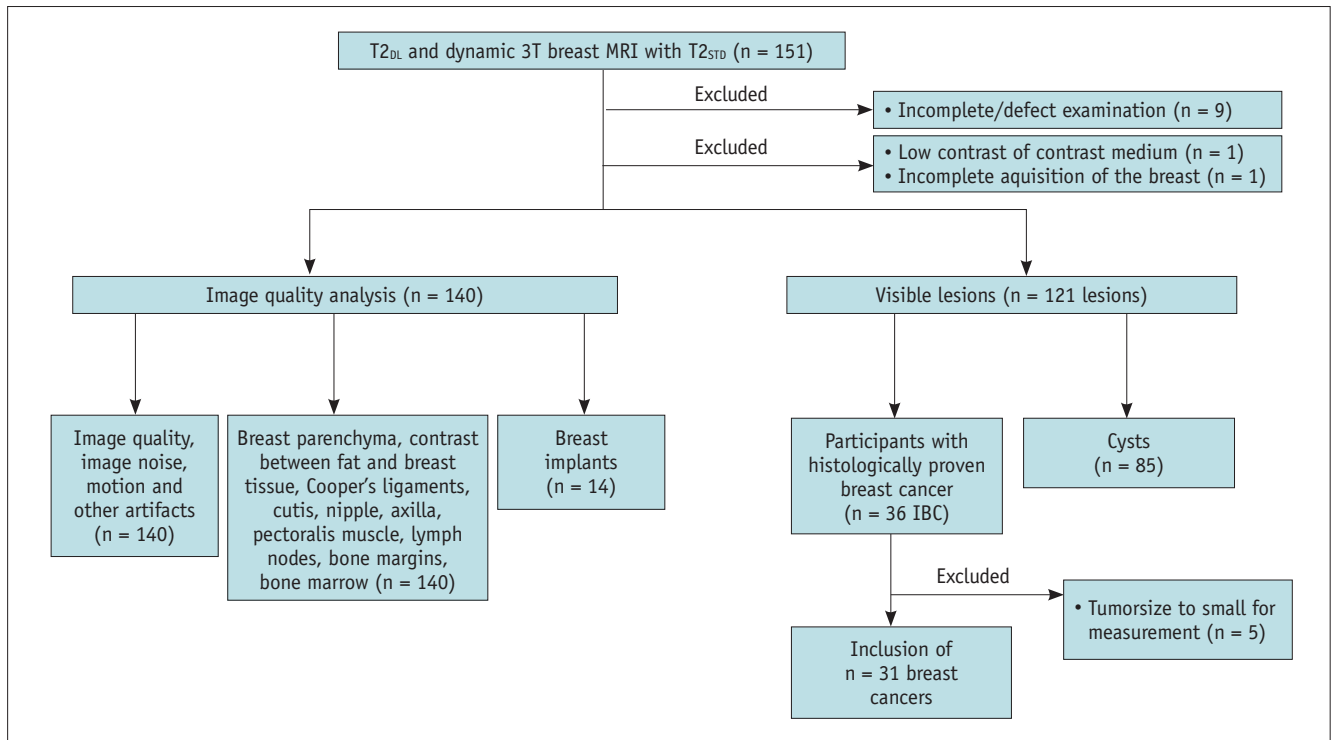


Fig. 1. Flowchart depicting patient inclusion and allocation to subgroups for the analysis. T2_{DL} = deep learning reconstructed T2-weighted fast spin-echo Dixon sequence with super-resolution, T2_{STD} = standard T2-weighted fast spin-echo Dixon sequence, IBC = invase breast cancer

differed (T2_{DL}: 305 × 576, 0.3 × 0.3 × 3.0 mm³ (interpolated) vs. T2_{STD}: 576 × 576, 0.6 × 0.6 × 3.0 mm³). Changes in phase oversampling (T2_{DL}: 75%, T2_{STD}: 30%) and phase resolution (T2_{DL}: 100%, T2_{STD}: 53%) were applied to accelerate the DL sequence. All other sequence parameters were set identically (Table 1).

DL-Based Image Reconstruction

The employed DL-based image reconstruction comprised two sequential, separate processing steps, both trained on clinical 1.5T and 3T scanners (MAGNETOM, Siemens Healthcare). First, images were reconstructed from k-space data using an architecture inspired by variational networks [18,21]. The model received undersampled k-space data as well as coil sensitivity maps estimated from calibration scans as input. It then generated an image through multiple iterations that alternated between data consistency updates and hierarchical down-up networks for image regularization. The architecture was implemented offline and trained in a supervised manner using approximately 25000 fully sampled images acquired with different contrasts in various body regions.

In the second step, the obtained images were interpolated using a DL-based SR algorithm based on a residual dense network [21]. The algorithm performed an initial upsampling

by a factor of two in both image dimensions in-plane and was trained in a supervised manner using approximately 14000 images acquired with different contrasts in different body regions. After the DL-based SR, the obtained images were finally interpolated to the target resolution using conventional sinc-interpolation. For both processing steps, the determined network parameters were exported and integrated into a research application for prospective use in the scanner's reconstruction pipeline.

Quantitative Image Analysis

For quantitative image analysis, region-of-interest (ROI) were placed by a radiologist (C.W.; 6 years' experience in breast imaging) in breast tissue, fat tissue, and air using in-house developed image analysis software (<https://www.nora-imaging.com>), allowing placement of ROI in the exact same locations in the spatially co-registered T2_{DL} sequence. SNR was calculated using the following equation:

$$\text{SNR}_{\text{Breast tissue}} = \text{Mean SI}_{\text{Breast tissue}} / \text{SD}_{\text{Air}} \text{ and}$$

$$\text{SNR}_{\text{Fat tissue}} = \text{Mean SI}_{\text{Fat tissue}} / \text{SD}_{\text{Air}}.$$

In addition, the contrast-to-noise ratio (CNR) in breast cancers was calculated using the following formula:

$$\text{CNR}_{\text{Breast cancers}} = \frac{|\text{MeanSI}_{\text{Surrounding breast tissue}} - \text{MeanSI}_{\text{Breast cancers}}|}{\text{SD}_{\text{Air}}}.$$

Table 1. Acquisition parameters of the deep learning T2_{DL} and the conventional T2_{STD} in comparison

Characteristic	T2 _{DL}	T2 _{STD}
FOV, mm ²	340 × 340	
Matrix size	305 × 576	576 × 576
Number of slices	55	
Slice thickness, mm	3	
Resolution, mm ³	0.3 (i) × 0.3 (i) × 3.0	0.6 × 0.6 × 3.0
TR, ms	6000	
TE, ms	101	
Flip angle, °	151	
Phase oversampling, %	75	30
Phase resolution, %	53	100
Fat saturation technique	Dixon	
Turbo factor	19	
Echo trains per slice	8	21
Averages	1	
Concatenations	2	
Acceleration factor	4	2
Reconstruction	Deep learning unrolled network	GRAPPA
Interpolation mode	Deep learning super-resolution network	None
Acquisition time, s	110	266

T2_{DL} = deep learning reconstructed T2-weighted fast spin-echo Dixon sequence with super resolution, T2_{STD} = standard T2-weighted fast spin-echo Dixon sequence, FOV = field of view, (i) = interpolated, TR = repetition time, TE = echo time, GRAPPA = generalized autocalibrating partially parallel acquisition

Qualitative Image Analysis

To assess qualitative image quality, in-phase and water-images of the T2-w Dixon sequences (T2_{DL}, T2_{STD}) were independently rated by two radiologists with 6 (C.W.) and 12 years (J.N.) of experience in breast imaging. T2_{STD} and T2_{DL} were shown in direct intra-individual comparison in random order on diagnostic monitors in a blinded fashion. Image noise, motion, and other artifacts were assessed using Likert scales ranging from 1 (none), 2 (minimal), 3 (moderate) to 4 (very strong). Reading scores of 1 and 2 were considered sufficient for clinical use. Readers also independently assessed, using Likert scales ranging from 1 (non-diagnostic), 2 (poor), 3 (moderate), 4 (good), to 5 (excellent), overall image quality; visibility of breast parenchyma; contrast between breast tissue and fat; sharpness of Cooper's ligaments, cutis, nipple, pectoralis muscle, breast implants (if applicable), axilla, lymph nodes, bone margins, and bone marrow; as well as conspicuity, sharpness/margins, and microstructure of cysts and breast cancers. Reading scores of 4 and 5 were considered sufficient

for clinical use. The degree of suspicion for malignancy was also recorded for breast cancers, ranging from 1 (no), 2 (unlikely), 3 (possible), 4 (probable), to 5 (almost certain). Cysts were defined by a strong and homogenous T2w-hyperintense signal with sharp margins. In the case of multiple cysts, only the largest cyst was analyzed.

To evaluate readers' preferences for the sequence type, a split view was selected on a diagnostic monitor, and both sequences of each participant (T2_{DL}, T2_{STD}) were presented side-by-side in a blinded and randomized order, so that readers did not know which sequence was presented on the left or right of the split view.

Statistical Analysis

Normal distribution was tested using the Shapiro-Wilk test. Continuous data are presented as means ± standard deviations (SD) for normally distributed data and median ± interquartile ranges (IQR) for non-normally distributed data, unless otherwise stated. Paired samples *t*-test and Wilcoxon Signed-Rank tests were used to test for differences. Chi-square test was used to compare readers' preferences in side-by-side comparisons. Inter-reader reliability analysis was performed using weighted Cohen's Kappa (κ). Agreement was interpreted according to the definition by Landis and Koch [22]. Statistical analyses were performed using SPSS 29.0 (IBM Corp., Armonk, NY, USA). Two-sided *P*-values of <0.05 were considered statistically significant.

RESULTS

Study Cohort

Of the 237 participants who were offered participation in the study, 151 women agreed to participate and gave written informed consent prior to the examination. Eleven participants were excluded from the analysis: nine due to incomplete MRI scans, one due to a technical coil failure, and one due to incomplete breast coverage. The final cohort consisted of 140 women with a mean age ± SD of 52 ± 14 years. A total of 140 MRI examinations were analyzed for image quality features. Eighty-five cysts and 31 breast cancers were analyzed by the readers. The average size of cysts was 0.9 ± 0.9 cm (range: 0.2–4.4 cm). Five patients were excluded from the breast cancer analysis because the tumors were too small for sufficient measurements, defined as diameters less than 3 mm or due to locations close to a marker clip with susceptibility artifacts. The average size of breast cancers was 2.8 ± 2.2 cm (range: 0.3–9.0 cm). See

Table 2. Patient and lesion characteristics

Characteristic	Data
Patient (n = 140)	
Age, yrs	52 ± 14 (range, 24–82)
Total number of included participants	140
Reason for examination	
Diagnostic confirmation	30/140
Screening	21/140
High risk screening	51/140
Staging	32/140
Follow-up	6/140
Menopausal status	
Premenopausal	58/140
Postmenopausal	82/140
Breast density	
A (almost entirely fatty)	10/140
B (scattered fibroglandular tissue)	31/140
C (heterogeneously dense tissue)	48/140
D (extremely dense tissue)	41/140
Silicone implants	14/140 (unilateral: 10, bilateral: 4)
Breast cancer (n = 31)	
Histopathological finding	
NST (no special type)	20/31
NST + DCIS	4/31
DCIS	1/31
Lobular cancer	3/31
Mucinous cancer	1/31
Inflammatory cancer	1/31
Sarcoma	1/31
TNM (8th ed), T	
pTis	1/31
cT1	17/31
cT2	9/31
cT3	2/31
cT4	2/31
Histologic grade	
G1	2/31
G2	18/31
G3	11/31
TNM (8th ed), N	
N0	26/31
N1	5/31
TNM (8th ed), M	
M0	28/31
M1	3/31
Esterogene receptor	
Positive	19/31
Negative	12/31

Table 2. Patient and lesion characteristics (continued)

Characteristic	Data
Progesterone receptor	
Positive	18/31
Negative	13/31
HER2	
Positive	9/31
Negative	22/31
Ki-67	
<10%	4/31
>10%	27/31

Data are given in number of participants or mean ± standard deviation values.

NST = no special type, DCIS = ductal carcinoma in situ, pTis = ductal carcinoma in situ without invasive carcinoma, HER2 = human epidermal receptor, Ki-67 = proliferation index

Figure 1 for a description of the study cohort and Table 2 for detailed tumor characteristics.

Acquisition Time

With a 58% reduction, the acquisition time of T2_{DL} was significantly shorter compared to T2_{STD} (T2_{DL}: 110 s ± 0 vs. T2_{STD}: 266 s ± 0), corresponding to a potential saving of 156 seconds in T2_{DL} (Fig. 2).

Quantitative Image Analysis

The SNR of breast and fat tissue in T2_{DL} was significantly higher compared to T2_{STD} ($P < 0.001$). Breast cancers showed significantly higher mean CNR in T2_{DL} compared to T2_{STD} ($P < 0.001$) (Table 3, Fig. 3).

Qualitative Image Analysis

T2_{DL} was superior to T2_{STD} in terms of image noise, artifacts, and overall image quality ($P < 0.001$) (Table 4, Fig. 4, Supplementary Fig. 1). T2_{DL} was superior to T2_{STD} for all anatomical structures ($P \leq 0.008$) except for bone marrow, for which both readers reported lower scores for T2_{DL} compared to T2_{STD} ($P < 0.001$). Further details, including κ values and examples, are provided in Table 4 and Figure 4.

Conspicuity, sharpness, and microstructure of cysts were rated significantly higher in T2_{DL} compared to T2_{STD} ($P < 0.001$) (Table 4). Diagnostic confidence in the assessment of cysts was also rated significantly higher in T2_{DL} compared to T2_{STD} ($P < 0.001$) (Table 4, Fig. 5, Supplementary Fig. 2A).

Breast cancers showed significantly higher scores in T2_{DL} compared to T2_{STD} for conspicuity, margins, and microstructure ($P \leq 0.002$) (Table 4). Diagnostic confidence

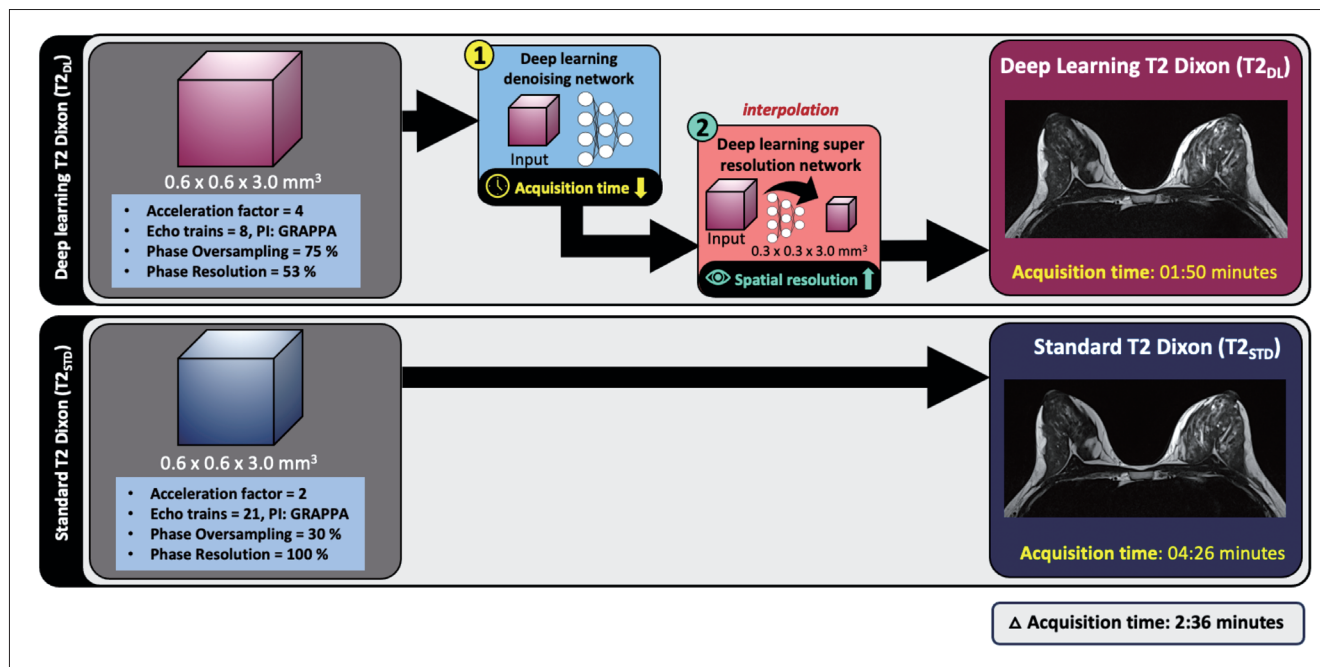


Fig. 2. Sequences and networks. Utilized T2-w MRI sequences and reconstruction workflow. Illustration of the sequences and DL networks used in the study. The upper box demonstrates the DL-reconstructed $T2_{DL}$, resulting in an interpolated spatial resolution of $0.3 \times 0.3 \times 3 \text{ mm}^3$ after the two DL networks (denoising network [1, yellow] and the super-resolution network [2, turquoise] are applied to the k-space data. The lower box shows the conventional T2-w Dixon sequence ($T2_{STD}$) with a spatial resolution of $0.6 \times 0.6 \times 3.0 \text{ mm}^3$. T2-w = T2-weighted, DL = deep learning, $T2_{DL}$ = deep learning reconstructed T2-weighted Dixon with super-resolution, $T2_{STD}$ = standard T2-weighted fast spin-echo Dixon sequence, PI = parallel imaging, GRAPPA = generalized autocalibrating partially parallel acquisition

Table 3. SNR and CNR

	$T2_{DL}$		$T2_{STD}$		<i>P</i>
	Mean	SD	Mean	SD	
SNR breast tissue (n = 140)	50.9	26.1	40.1	19.5	<0.001
SNR fat tissue (n = 140)	155.6	51.3	113.5	36.1	<0.001
CNR breast cancers (n = 31)	99.1	52.7	65.9	33.2	<0.001

SNR = signal-to-noise ratio, CNR = contrast-to-noise ratio, $T2_{DL}$ = deep learning reconstructed T2-weighted Dixon with super-resolution, $T2_{STD}$ = standard T2-weighted fast spin-echo Dixon sequence, SD = standard deviation

for breast cancers was significantly higher for $T2_{DL}$ only for reader 2 ($P = 0.031$). Further details and examples are given in Table 4, Supplementary Figure 2B, and Figure 6. A sub-analysis of small lesions ($\leq 1 \text{ cm}$) showed consistent results (Supplementary Tables 1, 2).

When the readers compared both sequences side by side, both perceived significantly better overall image quality in $T2_{DL}$ compared to $T2_{STD}$ (reader 1: 130/140 cases, reader 2: 137/140 cases; both $P < 0.001$). In only a few cases (reader 1: 10/140; reader 2: 3/140), there was no noticeable difference in image quality between the two sequence types, or $T2_{STD}$ was preferred (Figs. 4-6).

DISCUSSION

In this prospective study, our results indicate that $T2_{DL}$ for breast MRI substantially accelerated acquisition time while improving SNR, CNR of breast cancers, and image quality compared to $T2_{STD}$. We also observed fewer motion artifacts, less image noise, and improved lesion conspicuity, visibility of microstructure, and increased edge sharpness in cysts and breast cancers. Diagnostic confidence in $T2_{DL}$ increased for cysts and remained the same for breast cancers, with no loss of morphological information. These findings support the feasibility of DL reconstruction for routine clinical practice.

Our study demonstrates that applying DL networks, in combination with modified sequence parameters and parallel

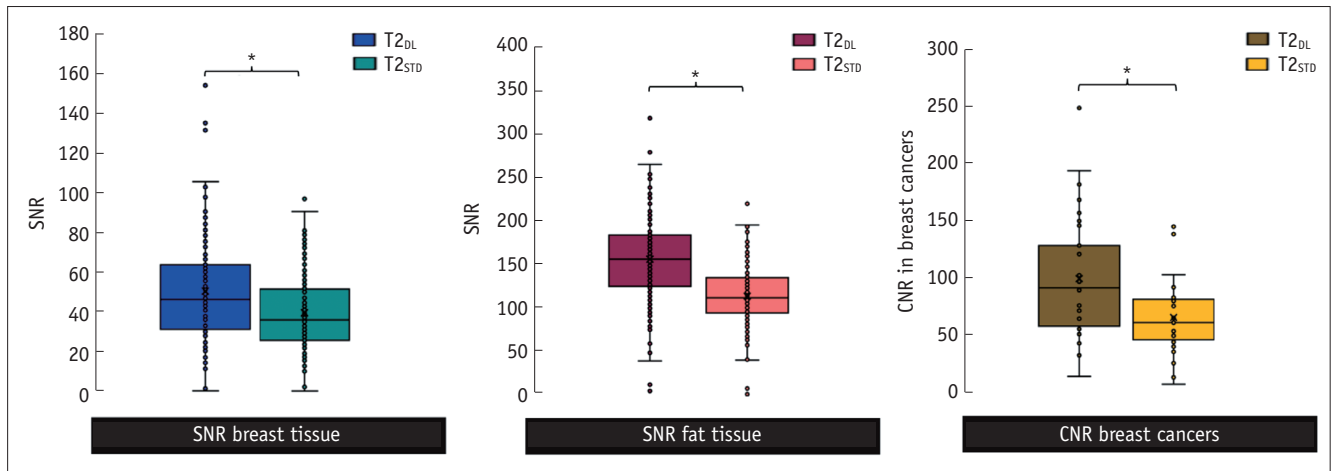


Fig. 3. Quantitative image quality analysis of breast tissue, fat tissue, and breast cancer. SNR of breast tissue and fat tissue, and CNR of breast cancers for conventional T2 Dixon (T2_{STD}) and T2_{DL}. T2_{DL} showed significantly higher SNR for breast and fat tissue as well as higher CNR in breast cancers. *Indicates statistically significant differences between both sequence types for each category, $P < 0.001$. SNR = signal-to-noise ratio, CNR = contrast-to-noise ratio, T2_{STD} = standard T2-weighted fast spin-echo Dixon sequence, T2_{DL} = deep learning reconstructed T2-weighted Dixon with super-resolution

imaging techniques, improved image quality while reducing acquisition time by 58%. Our results align with studies reporting shorter acquisition times for DL T2-w FSE of the breast [1], spine [23], or prostate MRI [3,4]. Even though the Dixon method has a longer examination time than standard T2w sequences [13], the acquisition of four contrasts offers diagnostic advantages, and the Dixon technique allows improved fat suppression in 3T breast MRI [12].

Motion and other artifacts occurred less frequently in T2_{DL}. This finding is significant, as motion artifacts are the most common, occurring in up to 16% of cases due to the long repetition time of T2-w sequences [24] and are a major cause of reduced image quality [25]. Shorter scan times can effectively reduce motion artifacts. Although evidence on the influence of DL networks on motion artifacts in breast imaging is lacking, this effect has been reported for a combination of DL and CS [26]. Similar to our study, Bischoff et al. [26] applied a denoising and upscaling DL reconstruction to standard T2-w FSE, low-resolution T2-w FSE, and low-resolution CS T2-w FSE, and found significantly improved image sharpness with reduced artifacts, including motion, ringing, partial volume, and susceptibility artifacts. The effect of faster acquisition time leading to fewer motion artifacts is expected to be similar for DL-reconstructed images. This is further supported by a study on DL reconstructions of the shoulder, which reported reduced motion artifacts [27]. Faster acquisition may especially improve image quality in patients with movement associated with pain or non-compliance.

Allen et al. [1] reported significantly improved SNR, sharpness, and image quality for DL-reconstructed T2-w breast MRI. They compared standard and high-resolution T2-w sequences with their DL-reconstructed versions. Similar to our results, SNR and CNR were improved through the application of DL networks. This aligns with studies that reported no loss of SNR with DL reconstructions for MRI of the prostate [28] and brain [29] or improved SNR for the prostate [30] and abdomen [31]. Thus, DL reconstructions help compensate for the limitations of parallel imaging, which usually only applies up to factors between 2 and 4 without a loss of SNR proportional to the square root of acceleration [32]. Our findings corroborate that the loss of SNR caused by higher acceleration factors can effectively be compensated by the denoising effects of DL networks [3,4]. Additionally, breast cancers presented with improved SNR and CNR, which is relevant for morphological structures. A study in women with breast cancer combined DL reconstruction with CS at 3T MRI and also found an additional gain in CNR and image quality scores compared to conventional T2-w FSE [1].

Despite the similarities between studies, comparisons can only be estimative due to differing sequences, settings, and organ systems. Notably, aside from one study on a combination of CS and DL in T2-w FSE [33] and one study on a T2-w FSE [1], no comparable studies exist on breast MRI using DL reconstructions on T2-w FSE Dixon sequences.

Regarding overall improved image quality, our results in the qualitative analysis align with studies reporting improved

Table 4. Qualitative analysis of image quality

	T2 _{DL}			T2 _{STD}			P	
	R1 median (IQR)	R2 median (IQR)	Cohen's κ (R1, R2)	R1 median (IQR)	R2 median (IQR)	Cohen's κ (R1, R2)	P (T2 _{DL} vs. T2 _{STD})	P (T2 _{DL} vs. T2 _{STD})
Image quality features (n = 140)								
Image noise	1 (1-1)	1 (1-1)	0.421	2 (2-2)	2 (2-2)	0.481	<0.001	<0.001
Motion artifacts	1 (1-2)	1 (1-2)	0.512	2 (1-2)	2 (1-3)	0.621	<0.001	<0.001
Other artifacts	1 (1-1)	1 (1-1)	0.455	2 (2-2)	2 (2-2)	0.487	<0.001	<0.001
Overall image quality	5 (5-5)	5 (5-5)	0.492	4 (4-4)	4 (4-4)	0.558	<0.001	<0.001
Anatomical structures and implant (n = 140)								
Visibility of breast parenchyma	5 (5-5)	5 (5-5)	0.691	4 (4-4)	4 (4-4)	0.522	<0.001	<0.001
Contrast between breast tissue and fat	5 (4-5)	5 (5-5)	0.348	5 (4-5)	5 (4-5)	0.461	<0.001	<0.001
Sharpness of Cooper's ligaments	5 (5-5)	5 (5-5)	0.288	4 (4-4)	4 (4-4)	0.502	<0.001	<0.001
Sharpness of cutis	5 (5-5)	5 (5-5)	0.205	4 (4-4)	4 (4-4)	0.627	<0.001	<0.001
Sharpness of nipple	5 (5-5)	5 (5-5)	0.205	4 (4-4)	4 (4-4)	0.653	<0.001	<0.001
Sharpness of pectoralis muscle	5 (5-5)	5 (5-5)	0.133	4 (4-4)	4 (4-4)	0.495	<0.001	<0.001
Sharpness of breast implants	5 (5-5)	5 (5-5)	0.874	4 (4-4)	4 (4-4)	0.965	0.008	0.008
Sharpness of axilla	5 (5-5)	5 (5-5)	0.374	4 (4-4)	4 (4-4)	0.521	<0.001	<0.001
Sharpness of lymph nodes	5 (5-5)	5 (5-5)	0.209	4 (4-4)	4 (4-4)	0.472	<0.001	<0.001
Sharpness of bone margins	5 (5-5)	5 (5-5)	0.195	4 (4-4)	4 (4-4)	0.333	<0.001	<0.001
Sharpness of bone marrow	4 (4-4)	4 (4-4)	0.180	5 (5-5)	5 (5-5)	0.417	<0.001	<0.001
Cysts (n = 85)								
Conspicuity	5 (5-5)	5 (5-5)	0.491	5 (5-5)	4 (4-4)	0.613	<0.001	<0.001
Sharpness	5 (5-5)	5 (5-5)	0.641	4 (4-4)	4 (4-4)	0.650	<0.001	<0.001
Microstructure	5 (5-5)	5 (5-5)	0.414	4 (4-4)	4 (4-4)	0.554	<0.001	<0.001
Diagnostic confidence	5 (5-5)	5 (5-5)	0.851	5 (5-5)	5 (4-5)	0.457	<0.001	<0.001
Breast cancers (n = 31)								
Conspicuity	5 (4-5)	5 (3-5)	0.918	4 (3-4)	4 (3-5)	0.808	<0.001	0.002
Margins	5 (4-5)	5 (4-5)	0.889	4 (3-4)	4 (3-4)	0.837	<0.001	<0.001
Microstructure	5 (3-5)	5 (4-5)	0.853	4 (3-4)	4 (2-4)	0.690	<0.001	<0.001
Diagnostic confidence	5 (3-5)	5 (3-5)	0.795	4 (3-5)	5 (3-5)	0.754	0.160	0.031
Suspicion for malignancy	5 (3-5)	5 (4-5)	0.726	5 (3-5)	5 (3-5)	0.746	0.125	0.500

Note that for image noise and motion and other artifacts, Likert scales ranged from 1 (none), 2 (minimal), 3 (moderate) to 4 (very strong) with reading scores of 1 and 2 considered sufficient for clinical use. The rate for malignancy for breast cancers was rated according to the following scale: 1 (no), 2 (unlikely), 3 (possible), 4 (probable), 5 (almost certain). For all other items Likert scales ranged from 1 (non-diagnostic), 2 (poor), 3 (moderate), 4 (good) to 5 (excellent), and reading scores of 4 and 5 were considered sufficient for clinical use. Data are given median with IQR in parenthesis. Interreader-reliability is specified in Cohen's κ. κ ≤ 0.20 corresponds to slight, 0.20 < κ ≤ 0.40 to fair, 0.40 < κ ≤ 0.60 to moderate, 0.60 < κ ≤ 0.80 to substantial, and 0.80 < κ ≤ 1.00 to almost perfect agreement between readers. Two-sided P-values were applied.

IQR = interquartile range, T2_{DL} = deep learning reconstructed T2-weighted Dixon with super-resolution, T2_{STD} = standard T2-weighted fast spin-echo Dixon sequence, R1 = reader 1, R2 = reader 2

image quality scores [1,33]. Other studies on breast MRI have focused on diffusion-weighted imaging [34-36], with only two examining standard T2-w imaging [1]. Far more studies have investigated other organ systems, finding improved image quality characteristics of DL-reconstructed sequences across various networks (denoising alone, SR alone, and combined denoising and SR). This has been demonstrated for T2-w imaging in the pancreas [37], musculoskeletal system

[38], prostate [26,39], and brain [40]. For T2-w imaging with DL reconstruction of the female pelvis in 3T MRI, reader preference and image quality were proven non-inferior compared to the standard T2-w turbo spin echo sequence [41]. Moreover, sequence interchangeability has been demonstrated for cervical and lumbar spine MRI features [23,42]. Compared to other studies, ours included different anatomical regions of the breast and axilla, along with numerous features

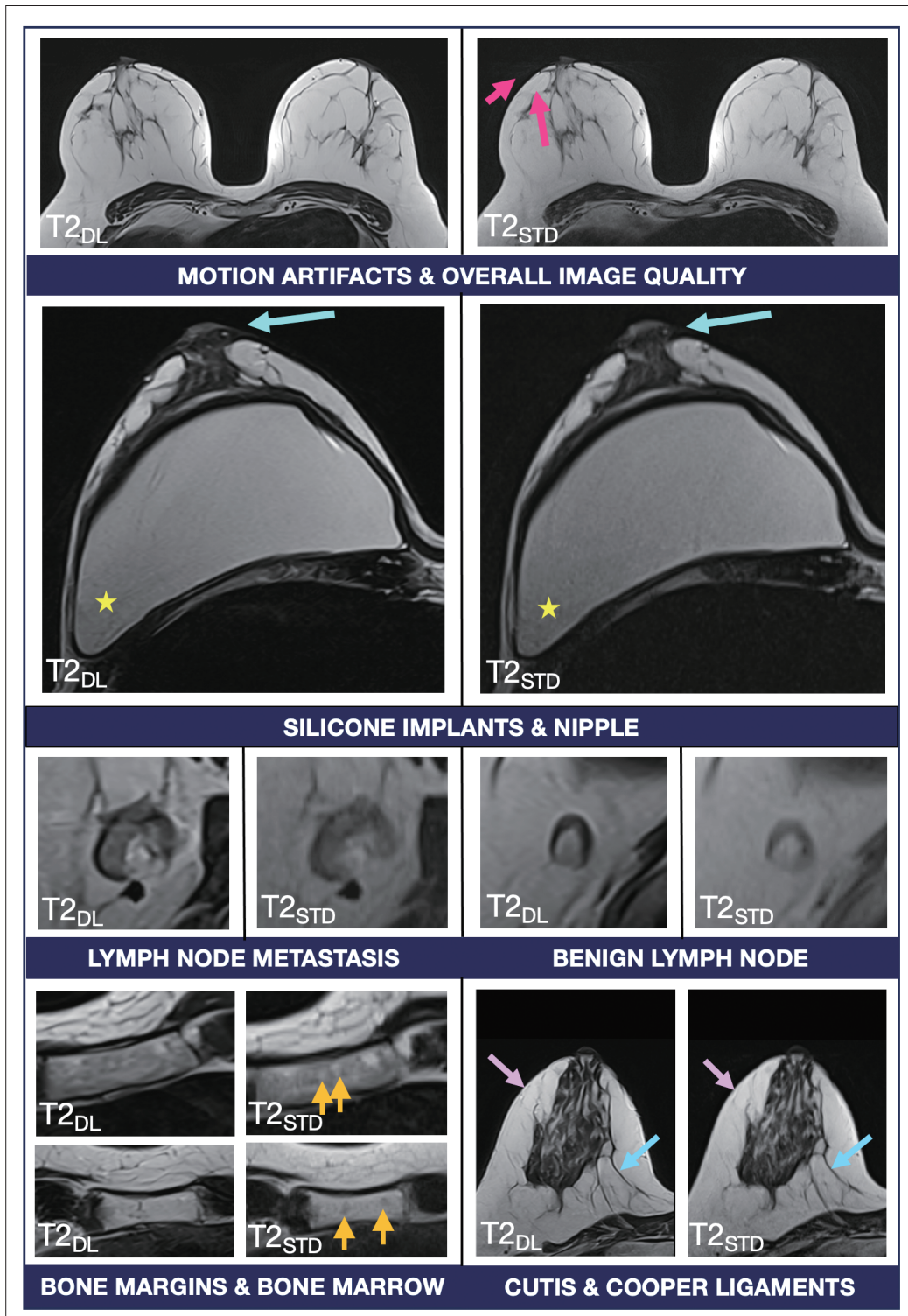


Fig. 4. Comparisons of image quality in deep learning reconstructed and standard breast MRI. The figure shows axial planes of the T2_{DL} on the left in comparison to the T2_{STD} on the right side for different anatomical regions and structures. Note the significantly improved image quality of anatomical structures and findings. The upper row shows a lymph node metastasis on the left and a benign lymph node on the right, each with improved sharpness in T2_{DL}. Motion artifacts (pink arrows) are more prominent in the T2_{STD} sequence. The yellow star demonstrates stronger noise in silicone implants in T2_{STD} compared to T2_{DL}. Sharpness of the nipples (blue arrows), cutis (violet arrows), and Cooper's ligaments (blue arrows, lower row) is improved in T2_{DL}. Notably, opposite results are seen for bone marrow (orange arrows), with sharper delineation of bone marrow structures in T2_{STD} compared to improved sharpness of bone margins in T2_{DL}. T2_{DL} = deep learning reconstructed T2-weighted Dixon with super-resolution, T2_{STD} = standard T2-weighted fast spin-echo Dixon sequence

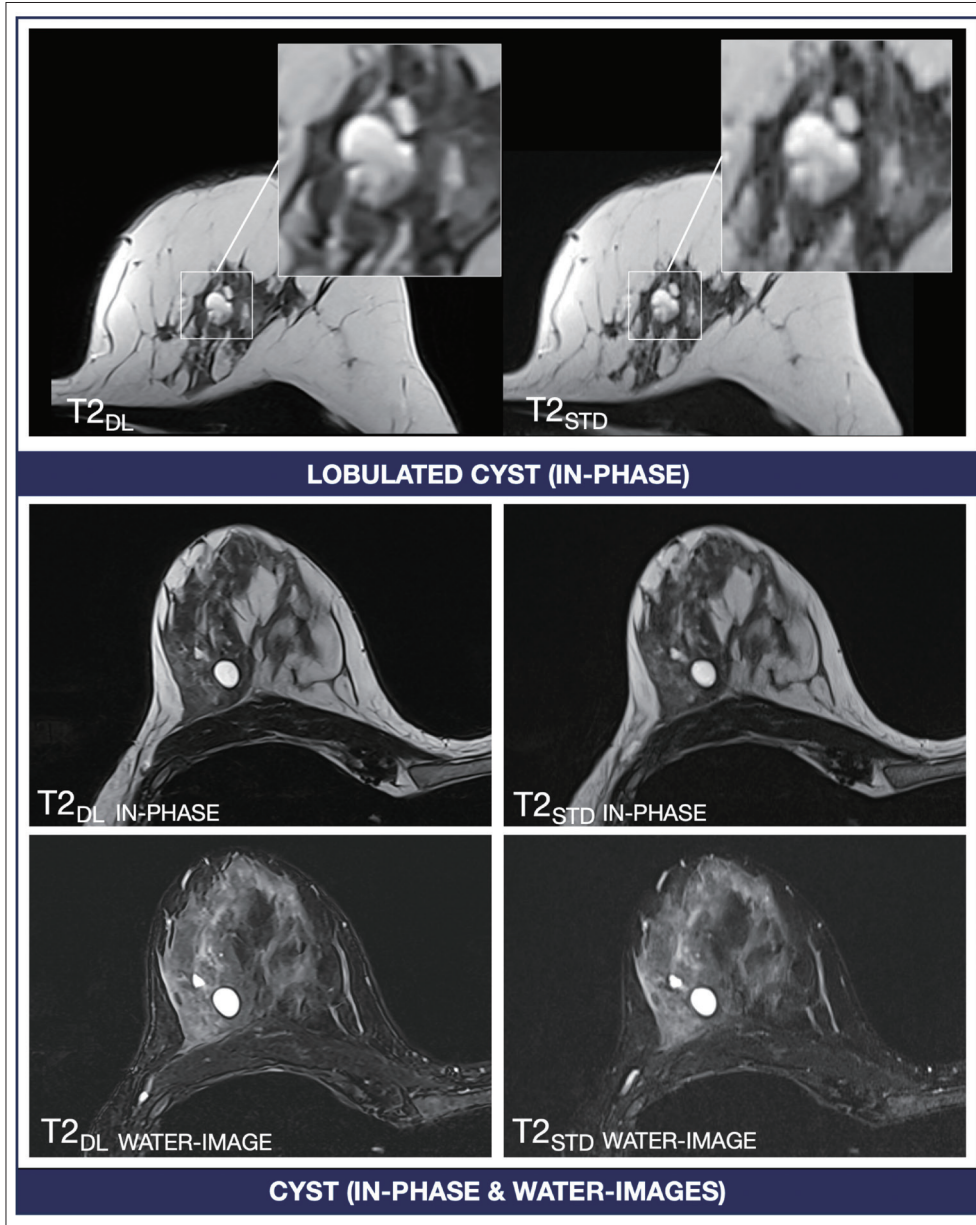


Fig. 5. Comparisons of image quality of DL reconstructed T2-w images and standard T2-w images with visible cysts including in-phase and water-images. The figure shows axial planes of $T2_{DL}$ on the left and $T2_{STD}$ on the right side, showing a lobulated cyst in the upper row and a simple cyst in the lower rows, including comparisons between in-phase and water images of the T2-w Dixon sequence. Note the increased sharpness of cysts in all DL reconstructed images. DL = deep learning, T2-w = T2-weighted, $T2_{DL}$ = deep learning reconstructed T2-weighted Dixon with super-resolution, $T2_{STD}$ = standard T2-weighted fast spin-echo Dixon sequence

such as the visibility of breast implants, allowing a precise evaluation of image quality in specific examination areas after applying DL networks. The improved scores in $T2_{DL}$ could result from edge-enhancing effects from the SR network and the doubled spatial resolution after acquiring only half the spatial resolution. The resulting higher SNR is smoothed by denoising effects, leading to an overall improved image quality. As no additional artifacts were reported, a cumulative

positive effect of combining both networks is assumed.

However, we observed inferior results for bone marrow in $T2_{DL}$. We suspect that the smoothing effects of SR reconstruction are responsible, as the heterogeneous structure of active bone marrow may be more susceptible to loss of structural details. It is difficult to draw causal inferences, so it remains unclear whether bone marrow is more susceptible to distortion in DL reconstructions than

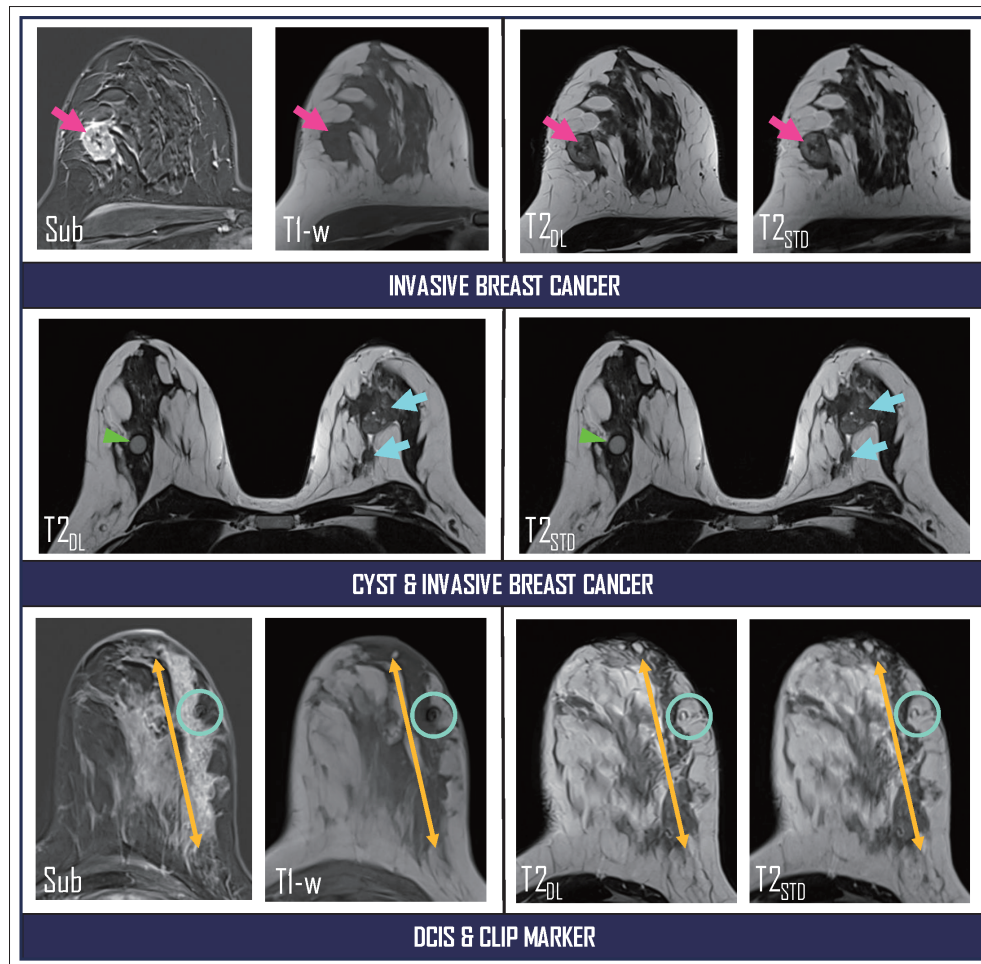


Fig. 6. Comparisons of image quality in deep learning reconstructed T2-w images and standard T2-w breast MRI in cases with visible masses and non-mass enhancement. The figure shows axial planes of the $T2_{DL}$ on the left and the $T2_{STD}$ on the right side for invasive breast cancer in the upper row (pink arrows), for invasive breast cancer (blue arrows, left breast) and a cyst (green arrowheads, right breast) in one patient in the middle row, and for DCIS (yellow bidirectional arrows) and a clip marker (blue ring) in the lower row. Subtraction images from the dynamic scan and T1-w images are also shown for the case in the upper and lower rows to demonstrate the findings in more detail. Note the increased sharpness of anatomical structures, cysts, and breast cancers in all images. $T2_w$ = T2-weighted, $T2_{DL}$ = deep learning reconstructed T2-weighted Dixon with super-resolution, $T2_{STD}$ = standard T2-weighted Dixon, DCIS = ductal carcinoma in situ, T1-w = T1-weighted, Sub = subtraction image from the first post-contrast dynamic scan

other anatomical structures. Consequently, $T2_{DL}$ might not be robust for supplementary assessment of bone marrow pathologies in breast MRI. Similar observations were reported in a study on the lumbar spine [2], but further studies focused on musculoskeletal applications of algorithms may be warranted.

The qualitative analysis showed that cysts were rated higher on $T2_{DL}$ for conspicuity, sharpness, microstructure, and diagnostic confidence. Our results are similar to those of Allen et al. [1], who evaluated DL T2-w FSE on 3T breast MRI and found improved sharpness for cysts and anatomical structures. Breast cancers also had higher quality scores in $T2_{DL}$ in our study, though the degree of

superior ratings and data dispersion was lower, particularly for conspicuity compared to cysts. This can be explained by the lower signal intensity and contrast of cancers in T2-w imaging compared to the very high signal of cysts. While an increase in detection rates was not expected, improved sharpness and microstructure could prove helpful for further lesion analysis, such as characterizing septa or irregularly shaped lesions, and likely explain the improved diagnostic confidence for cysts observed in $T2_{DL}$. It is noteworthy that the sub-analysis of small lesions was robust only for cystic lesions ($n = 56$). In contrast, only a few breast cancers had diameters ≤ 1 cm ($n = 3$), which did not allow for sufficient statistical analysis. As small cysts did not significantly

affect the qualitative analysis scores, this underscores the value of improved image quality for small lesions.

Our results suggest the application of T2_{DL} in clinical practice. In times of limited scanner availability, both time- and cost-effectiveness are increasingly important to meet the growing demand for breast MRI [43-45]. A study by Kim et al. [28] evaluated even further acceleration with a time reduction of up to 76%, finding that SNR did not differ between the most accelerated low-resolution DL sequence (52 s) and the conventional sequence (212 s), while contrast was higher in the conventional T2-w sequence [28]. As an outlook, a large reduction in acquisition time for T2-w could be useful for personalized abbreviated protocols [16,46]. Further sequence development and studies are needed to determine whether T2-w signal can be preserved after massive acquisition time reductions.

Limitations of this study include that it was performed only on a 3T scanner. The use of CS or simultaneous multi-slice techniques was not implemented, though there is evidence that these can further improve image quality [33]. The DL networks were not analyzed separately to investigate the effects of the denoising and SR networks independently. This may make it difficult to attribute specific effects to each network. The reduced scan time of T2_{DL} is not solely due to the acceleration of the parallel imaging technique and was partly due to increasing phase oversampling, reducing phase resolution, and shortening echo trains per slice. Additionally, T1-w images were not evaluated in this protocol, as it was not part of the study design. Regarding the qualitative analysis, the edge-sharpening effect in T2_{DL} may have led to a learning effect in the readers, which could have influenced the results. Only a small number of breast cancers (n = 31) and no benign masses were analyzed, which may not represent the wide range of tumor morphologies. Furthermore, this study was exploratory, with no adjustment for multiple comparisons or clinically meaningful effect sizes. We provide preliminary data that need to be replicated in future studies.

In conclusion, this prospective comparative study demonstrates the potential of a DL-reconstructed T2-w Dixon sequence to replace the commonly used T2-w sequence in breast MRI. With benefits of 58% faster acquisition time, improved image quality, reduced motion artifacts, and better diagnostic confidence regarding cysts and breast cancers, the applied DL reconstruction is feasible for clinical application. It could increase patient comfort and address the time- and cost-effectiveness of breast MRI.

Supplement

The Supplement is available with this article at <https://doi.org/10.3348/kjr.2023.1303>.

Availability of Data and Material

The datasets generated or analyzed during the study are available from the corresponding author on reasonable request.

Conflicts of Interest

Ralph Strecker, Marcel Dominic Nickel and Elisabeth Weiland are employees of Siemens Healthineers and work in the department for MR Application Predevelopment. Ralph Strecker is an employee of EMEA Scientific Partnerships for Siemens Healthineers and works as a collaboration manager. Employees of Siemens Healthineers had no control over the data at any time and provided technical information only. None of the other authors declare any conflict of interest, including Caroline Wilpert, who was in charge of all data at any given time point.

Author Contributions

Conceptualization: Caroline Wilpert, Jakob Neubauer, Hannah Schneider, Marisa Windfuhr-Blum. Data curation: Hannah Schneider, Alexander Rau, Caroline Wilpert, Jakob Neubauer. Formal analysis: Caroline Wilpert, Jakob Neubauer, Maximilian Frederic Russe, Jakob Weiss. Investigation: Caroline Wilpert, Jakob Neubauer, Hannah Schneider, Maximilian Frederic Russe. Methodology: Caroline Wilpert, Jakob Neubauer, Matthias Benndorf, Benedict Oerther, Jakob Weiss. Project administration: Caroline Wilpert, Jakob Neubauer, Hannah Schneider, Matthias Benndorf, Jakob Weiss, Fabian Bamberg. Resources: Ralph Strecker, Marcel Dominic Nickel, Elisabeth Weiland. Software: Alexander Rau. Supervision: Caroline Wilpert, Jakob Neubauer, Matthias Benndorf, Jakob Weiss, Fabian Bamberg. Validation: Caroline Wilpert, Jakob Neubauer, Fabian Bamberg, Marisa Windfuhr-Blum. Visualization: Caroline Wilpert, Alexa Haeger. Writing—original draft: Caroline Wilpert, Jakob Neubauer. Writing—review & editing: all authors.

ORCID IDs

Caroline Wilpert

<https://orcid.org/0000-0003-2375-2478>

Hannah Schneider

<https://orcid.org/0009-0005-8940-6182>

Alexander Rau

<https://orcid.org/0000-0001-5881-6043>

Maximilian Frederic Russe

<https://orcid.org/0000-0003-3187-2429>

Benedict Oerther

<https://orcid.org/0000-0003-4267-3601>

Ralph Strecker

<https://orcid.org/0000-0002-8232-8952>

Marcel Dominic Nickel

<https://orcid.org/0000-0001-6141-5857>

Elisabeth Weiland

<https://orcid.org/0000-0001-7517-1291>

Alexa Haeger

<https://orcid.org/0000-0003-2927-4016>

Matthias Benndorf

<https://orcid.org/0000-0002-0407-1266>

Thomas Mayrhofer

<https://orcid.org/0000-0001-6287-5185>

Jakob Weiss

<https://orcid.org/0000-0002-3879-0568>

Fabian Bamberg

<https://orcid.org/0000-0002-7460-3942>

Jakob Neubauer

<https://orcid.org/0000-0001-9388-0219>

Funding Statement

None

REFERENCES

- Allen TJ, Henze Bancroft LC, Unal O, Estkowski LD, Cashen TA, Korosec F, et al. Evaluation of a deep learning reconstruction for high-quality T2-weighted breast magnetic resonance imaging. *Tomography* 2023;9:1949-1964
- Berkarda Z, Wiedemann S, Wilpert C, Strecker R, Koerzdoerfer G, Nickel D, et al. Deep learning reconstructed T2-weighted Dixon imaging of the spine: impact on acquisition time and image quality. *Eur J Radiol* 2024;178:111633
- Gassenmaier S, Afat S, Nickel D, Mostapha M, Herrmann J, Othman AE. Deep learning-accelerated T2-weighted imaging of the prostate: reduction of acquisition time and improvement of image quality. *Eur J Radiol* 2021;137:109600
- Gassenmaier S, Afat S, Nickel MD, Mostapha M, Herrmann J, Almansour H, et al. Accelerated T2-weighted TSE imaging of the prostate using deep learning image reconstruction: a prospective comparison with standard T2-weighted TSE imaging. *Cancers (Basel)* 2021;13:3593
- Chazen JL, Tan ET, Fiore J, Nguyen JT, Sun S, Sneag DB. Rapid lumbar MRI protocol using 3D imaging and deep learning reconstruction. *Skeletal Radiol* 2023;52:1331-1338
- Herrmann J, Wessling D, Nickel D, Arberet S, Almansour H, Afat C, et al. Comprehensive clinical evaluation of a deep learning-accelerated, single-breath-hold abdominal HASTE at 1.5 T and 3 T. *Acad Radiol* 2023;30:93-102
- Afat S, Wessling D, Afat C, Nickel D, Arberet S, Herrmann J, et al. Analysis of a deep learning-based superresolution algorithm tailored to partial fourier gradient echo sequences of the abdomen at 1.5 T: reduction of breath-hold time and improvement of image quality. *Invest Radiol* 2022;57:157-162
- Kuhl CK, Klaschik S, Mielcarek P, Gieseke J, Wardelmann E, Schild HH. Do T2-weighted pulse sequences help with the differential diagnosis of enhancing lesions in dynamic breast MRI? *J Magn Reson Imaging* 1999;9:187-196
- Rahbar H, Partridge SC, DeMartini WB, Thursten B, Lehman CD. Clinical and technical considerations for high quality breast MRI at 3 tesla. *J Magn Reson Imaging* 2013;37:778-790
- Ma J. Dixon techniques for water and fat imaging. *J Magn Reson Imaging* 2008;28:543-558
- Dogan BE, Scoggins ME, Son JB, Wei W, Candelaria R, Yang WT, et al. American College of Radiology-compliant short protocol breast MRI for high-risk breast cancer screening: a prospective feasibility study. *AJR Am J Roentgenol* 2018;210:214-221
- Clauser P, Pinker K, Helbich TH, Kapetas P, Bernathova M, Baltzer PA. Fat saturation in dynamic breast MRI at 3 tesla: is the Dixon technique superior to spectral fat saturation? A visual grading characteristics study. *Eur Radiol* 2014;24:2213-2219
- Guerini H, Omoumi P, Guichoux F, Vuillemin V, Morvan G, Zins M, et al. Fat suppression with Dixon techniques in musculoskeletal magnetic resonance imaging: a pictorial review. *Semin Musculoskelet Radiol* 2015;19:335-347
- Dogan BE, Ma J, Hwang K, Liu P, Yang WT. T1-weighted 3D dynamic contrast-enhanced MRI of the breast using a dual-echo Dixon technique at 3 T. *J Magn Reson Imaging* 2011;34:842-851
- Mootz AR, Madhuranthakam AJ, Doğan B. Changing paradigms in breast cancer screening: abbreviated breast MRI. *Eur J Breast Health* 2019;15:1-6
- Grimm LJ, Soo MS, Yoon S, Kim C, Ghate SV, Johnson KS. Abbreviated screening protocol for breast MRI: a feasibility study. *Acad Radiol* 2015;22:1157-1162
- Kidoh M, Shinoda K, Kitajima M, Isogawa K, Nambu M, Uetani H, et al. Deep learning based noise reduction for brain MR imaging: tests on phantoms and healthy volunteers. *Magn Reson Med Sci* 2020;19:195-206
- Hammernik K, Klatzer T, Kobler E, Recht MP, Sodickson DK, Pock T, et al. Learning a variational network for reconstruction of accelerated MRI data. *Magn Reson Med* 2018;79:3055-3071
- Higaki T, Nakamura Y, Tatsugami F, Nakaura T, Awai K. Improvement of image quality at CT and MRI using deep learning. *Jpn J Radiol* 2019;37:73-80
- Antun V, Renna F, Poon C, Adcock B, Hansen AC. On instabilities of deep learning in image reconstruction and the potential costs of AI. *Proc Natl Acad Sci U S A* 2020;117:30088-30095

21. Zhang Y, Tian Y, Kong Y, Zhong B, Fu Y. Residual dense network for image super-resolution [accessed on September 8, 2024]. Available at: https://openaccess.thecvf.com/content_cvpr_2018/html/Zhang_Residual_Dense_Network_CVPR_2018_paper.html
22. Landis JR, Koch GG. The measurement of observer agreement for categorical data. *Biometrics* 1977;33:159-174
23. Almansour H, Herrmann J, Gassenmaier S, Afat S, Jacoby J, Koerzdoerfer G, et al. Deep learning reconstruction for accelerated spine MRI: prospective analysis of interchangeability. *Radiology* 2023;306:e212922
24. Fiaschetti V, Pistolesi CA, Funel V, Rascioni M, Claroni G, Della Gatta F, et al. Breast MRI artefacts: evaluation and solutions in 630 consecutive patients. *Clin Radiol* 2013;68:e601-e608
25. Kim SG, Drotman MB. *Artifacts in breast MRI*. In: Pinker K, Mann R, Partridge S, eds. *Advances in magnetic resonance technology and applications*. 5th ed. New York: Elsevier, 2022:33-48
26. Bischoff LM, Peeters JM, Weinhold L, Krausewitz P, Ellinger J, Katemann C, et al. Deep learning super-resolution reconstruction for fast and motion-robust T2-weighted prostate MRI. *Radiology* 2023;308:e230427
27. Hahn S, Yi J, Lee HJ, Lee Y, Lim YJ, Bang JY, et al. Image quality and diagnostic performance of accelerated shoulder MRI with deep learning-based reconstruction. *AJR Am J Roentgenol* 2022;218:506-516
28. Kim EH, Choi MH, Lee YJ, Han D, Mostapha M, Nickel D. Deep learning-accelerated T2-weighted imaging of the prostate: impact of further acceleration with lower spatial resolution on image quality. *Eur J Radiol* 2021;145:110012
29. Uetani H, Nakaura T, Kitajima M, Morita K, Haraoka K, Shinojima N, et al. Hybrid deep-learning-based denoising method for compressed sensing in pituitary MRI: comparison with the conventional wavelet-based denoising method. *Eur Radiol* 2022;32:4527-4536
30. Ueda T, Ohno Y, Yamamoto K, Murayama K, Ikedo M, Yui M, et al. Deep learning reconstruction of diffusion-weighted MRI improves image quality for prostatic imaging. *Radiology* 2022;303:373-381
31. Tanabe M, Higashi M, Yonezawa T, Yamaguchi T, Iida E, Furukawa M, et al. Feasibility of high-resolution magnetic resonance imaging of the liver using deep learning reconstruction based on the deep learning denoising technique. *Magn Reson Imaging* 2021;80:121-126
32. Yang RK, Roth CG, Ward RJ, deJesus JO, Mitchell DG. Optimizing abdominal MR imaging: approaches to common problems. *Radiographics* 2010;30:185-199
33. Yang F, Pan X, Zhu K, Xiao Y, Yue X, Peng P, et al. Accelerated 3D high-resolution T2-weighted breast MRI with deep learning constrained compressed sensing, comparison with conventional T2-weighted sequence on 3.0 T. *Eur J Radiol* 2022;156:110562
34. Wilpert C, Neubauer C, Rau A, Schneider H, Benkert T, Weiland E, et al. Accelerated diffusion-weighted imaging in 3 T breast MRI using a deep learning reconstruction algorithm with superresolution processing: a prospective comparative study. *Invest Radiol* 2023;58:842-852
35. Lee EJ, Chang YW, Sung JK, Thomas B. Feasibility of deep learning k-space-to-image reconstruction for diffusion weighted imaging in patients with breast cancers: focus on image quality and reduced scan time. *Eur J Radiol* 2022;157:110608
36. Wessling D, Gassenmaier S, Olthof SC, Benkert T, Weiland E, Afat S, et al. Novel deep-learning-based diffusion weighted imaging sequence in 1.5 T breast MRI. *Eur J Radiol* 2023;166:110948
37. Chaika M, Afat S, Wessling D, Afat C, Nickel D, Kannengiesser S, et al. Deep learning-based super-resolution gradient echo imaging of the pancreas: improvement of image quality and reduction of acquisition time. *Diagn Interv Imaging* 2023;104:53-59
38. Chaudhari AS, Fang Z, Kogan F, Wood J, Stevens KJ, Gibbons EK, et al. Super-resolution musculoskeletal MRI using deep learning. *Magn Reson Med* 2018;80:2139-2154
39. Tong A, Bagga B, Petrocelli R, Smereka P, Vij A, Qian K, et al. Comparison of a deep learning-accelerated vs. conventional T2-weighted sequence in biparametric MRI of the prostate. *J Magn Reson Imaging* 2023;58:1055-1064
40. Kim SH, Choi YH, Lee JS, Lee SB, Cho YJ, Lee SH, et al. Deep learning reconstruction in pediatric brain MRI: comparison of image quality with conventional T2-weighted MRI. *Neuroradiology* 2023;65:207-214
41. Lee EJ, Hwang J, Park S, Bae SH, Lim J, Chang YW, et al. Utility of accelerated T2-weighted turbo spin-echo imaging with deep learning reconstruction in female pelvic MRI: a multi-reader study. *Eur Radiol* 2023;33:7697-7706
42. Kashiwagi N, Sakai M, Tsukabe A, Yamashita Y, Fujiwara M, Yamagata K, et al. Ultrafast cervical spine MRI protocol using deep learning-based reconstruction: diagnostic equivalence to a conventional protocol. *Eur J Radiol* 2022;156:110531
43. Taneja C, Edelsberg J, Weycker D, Guo A, Oster G, Weinreb J. Cost effectiveness of breast cancer screening with contrast-enhanced MRI in high-risk women. *J Am Coll Radiol* 2009;6:171-179
44. Geuzinge HA, Bakker MF, Heijnsdijk EAM, van Ravesteyn NT, Veldhuis WB, Pijnappel RM, et al. Cost-effectiveness of magnetic resonance imaging screening for women with extremely dense breast tissue. *J Natl Cancer Inst* 2021;113:1476-1483
45. Mann RM, Kuhl CK, Moy L. Contrast-enhanced MRI for breast cancer screening. *J Magn Reson Imaging* 2019;50:377-390
46. Harvey SC, Di Carlo PA, Lee B, Obadina E, Sippo D, Mullen L. An abbreviated protocol for high-risk screening breast MRI saves time and resources. *J Am Coll Radiol* 2016;13(11S):R74-R80